CORA Cork Open Research Archive
Cartlann Taighde Oscailte Chorcaí

Title	Core/shell (Cu/Cu2O) nanotubes as high performance anode materials for Li-ion rechargeable batteries
Authors	Hasan, Maksudul;Chowdhury, Tamjid;Rohan, James F.
Publication date	2009-01-01
Original Citation	Hasan, M., Chowdhury, T. and Rohan, J. (2009) 'Core/Shell (Cu/Cu2O) Nanotubes as High Performance Anode Materials for Li-ion Rechargeable Batteries', ECS Transactions, 19(27), pp. 3-15. doi: 10.1149/1.3265864
Type of publication	Article (peer-reviewed)
Link to publisher's version	http://ecst.ecsdl.org/content/19/27/3 - 10.1149/1.3265864
Rights	© 2009 ECS - The Electrochemical Society
Download date	2026-11-07 07:17:55
Item downloaded from	https://hdl.handle.net/10468/7604

UCC
University College Cork, Ireland
Coláiste na hOllscoile Corcaigh

Core/Shell (Cu/Cu_2O) Nanotubes as High Performance Anode Materials for Li-ion Rechargeable Batteries

Maksudul Hasan, Tamjid Chowdhury and James F. Rohan

Tyndall National Institute, University College Cork, Lee Maltings, Cork, Ireland.

A direct electrodeposition technique for very high quality Cu nanotube arrays and subsequent conversion of the deposited Cu into Cu_2O has been developed. The Cu_2O nanotube arrays have high capacity, high cyclability and high rate capability. The cycling performance of Cu_2O nanotubes show a high level of structural integrity with capacity retention even after 94 cycles when cycled at 1.67 mA/cm^2. The outstanding electrochemical performance of the Cu_2O nanotubes comes from high surface area, easy infiltration of electrolytes, high electrical conductivity of Cu core support and structural integrity of the oxide shell active material. The Cu_2O nanotubes also eliminate the requirement of ancillary materials currently used in Li-ion batteries, such as carbon particles to increase conductivity. The easy fabrication and performance of Cu_2O nanotube arrays may make them suitable for next generation Li-ion batteries.

Introduction

One dimensional (1D) nanostructures have recently attracted much attention for potential applications in electronic and optoelectronic nanodevices as well as possible applications in the nanoscale energy storage/conversion devices (1-3) due to their unique physical properties that differ from the bulk materials. 1D nanostructures provide additional electrode surface area, to facilitate Li^+ insertion/de-insertion, short path lengths for electronic and Li^+ transport and thus higher charge/discharge rates (4). The development of nanoscale lithium-ion materials lies at the heart of new battery technologies that have higher Li^+ storage capacity and higher rate capability for charge and discharge. Recently, metal oxides of iron, cobalt and copper have attracted attention as anode materials for Li-ion batteries based on the novel reaction mechanism proposed by Tarascon et al (5). The reaction mechanism involves the compositional transformation of metal oxides to metal nanodomains dispersed in Li_2O during the charging process which regain the original composition during the discharging process. More recently, Tarascon et al., demonstrated the idea of the so called "conversion reactions" for 1D Fe_3O_4 nanorod structures (6). The reaction mechanism is different from the classical Li^+ insertion/de-insertion. High capacity and rate capability (for example, 80% capacity retention at 8 C rates) have been reported (6) using these nanorod arrays. Mesoporous Co_3O_4 nanorods of the same "conversion reactions" family have been synthesised by an ammonia-evaporation-induced method on various substrates such as Si wafer, glass slide, Cu or Ti foil, and polystyrene (7). Cu_2O has also attracted much interest among the "conversion reaction" oxide family members because of the high reversible capacity demonstrated (8). Cu_2O nanowires have been fabricated in anodised alumina oxide (AAO) templates by electrodeposition from a copper acetate/lactate bath with Cu as co-

deposit (9). The variation of local pH at the electrode surface during the deposition process results in the spontaneous potential oscillation and a Cu/Cu_2O composite deposit. However, the low efficiency of the bath has restricted its applications in Cu_2O nanowires deposition. Yang et al. oxidised Cu_2S nanowires under O_2 at elevated temperature and observed the formation of polycrystalline nanowires containing both Cu/Cu_2O (10).

In this paper, we will report a novel fabrication route to Cu nanotubes based on the direct electrodeposition into the pores of AAO template from an additive containing $CuSO_4$ bath and the subsequent conversion of the deposited Cu into Cu_2O. The novelty of the method is its simplicity and efficiency in producing a very high quality Cu nanotube array and conversion process. Hermann et al. synthesized Cu nanotubes via polycarbonate templates through a chemical reduction method for use as additives in the negative electrode of Ni-MH batteries (11). Another method involved sequential high temperature processing steps to achieve template assisted nanotube deposition (12). We will discuss here, the growth mechanism of Cu nanotubes under the influence of the additives by comparison with the more typical current density effect in electrodeposition. We will also present characterisation data for the Cu_2O by XRD, electrochemical performance as anode materials, and microstructure analysis by SEM to correlate with the Li cycling performance.

Experimental

Cu nanotubes were electrodeposited in anodised aluminium oxide (AAO) Anodisc membranes (Whatman, 19.5 mm diameter exposed, calculation based on exclusion of the polypropylene supporting ring, 60 μm thick and 10^9 pores per cm^2). The pore diameter was 250 to 300 nm. The complete fabrication process of Cu_2O nanotubes is illustrated in Fig. 1. A 500 nm thin layer of Ni conducting layer was deposited onto one side of AAO template by e-beam evaporation technique (Temescal FC-2000). The electrodeposition was carried out in a 0.24 M $CuSO_4$ (Fisher Scientific analytical reagent grade) and 1.8 M H_2SO_4 (Air products 96%) bath at room temperature with slow convection of the solution. The additives used in the bath were polyethylene glycol (PEG) (300 ppm) (SigmaUltra, mol. wt. 3350, powder) and Cl^- (50 ppm) as NaCl (BDH, analytical reagent grade). A constant current 40 mA was applied for Cu nanotubes electrodeposition using a potentiostat CHI instrument 660C in a two electrodes set up with Cu foil as the anode and Ni substrate in the pores of AAO as working electrode (cathode). The AAO template was mounted vertically in the cell facing the anode with the Ni seed layer on the opposite side open to the solution and the spacing between template and counter electrode was 1 cm. A Cu wire was connected to the Ni conducting side of the template by Ag conductive paint (Radionics Ltd. Ireland) left to dry overnight before use. The deposition rate was approximately 0.22 μm per minute. After electrodeposition the aluminium oxide template was stripped in 0.75 M NaOH (Sigma Aldrich) solution for 50 min, washed with plenty of water and dried in air. The electrodeposited Cu was converted to Cu_2O by oxygen plasma treatment (March Plasmod GCM 200) at 250 watt for 1 or 4.5 mins.

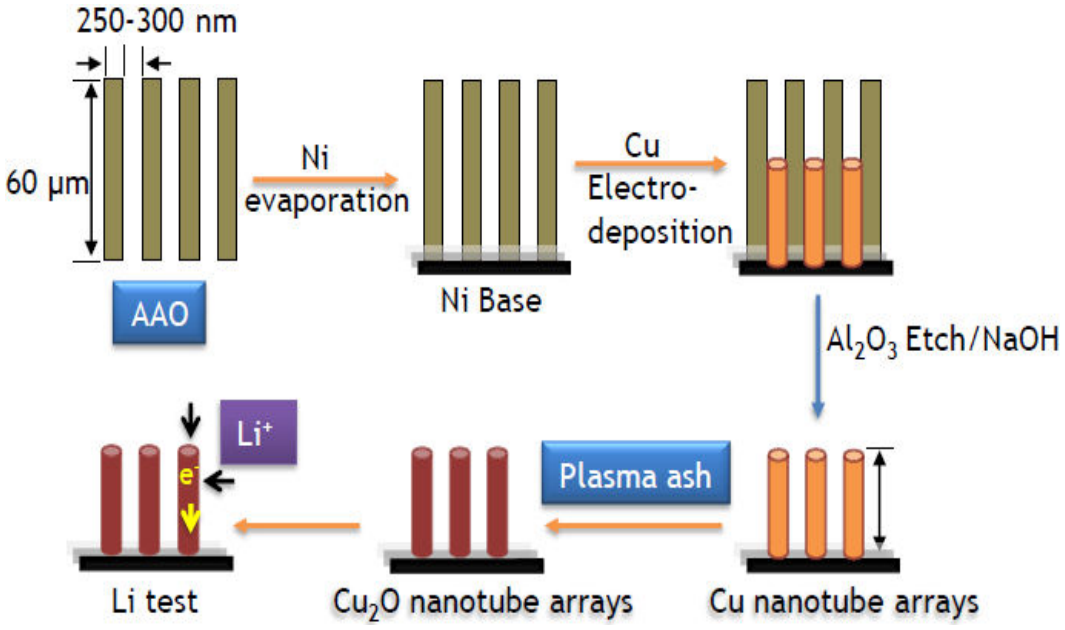


Figure 1. Schematic illustration of the synthesis process for high aspect ratio Cu_2O nanotube arrays.

The Li capacity test of Cu_2O nanotubes was performed by cyclic voltammetry and constant current experiments using a CHI 660C potentiostat and a three electrode set-up. The electrolyte consisted of 1M $LiPF_6$ in ethylene carbonate (EC)/diethyl carbonate (DEC) (1:1, in volume) purchased from Sigma-Aldrich. Lithium foil of 0.25 mm thickness (Aldrich) served as counter and reference electrodes. The cell was assembled in an argon-filled glove box where O_2 and H_2O were maintained at 0.1 ppm level. The capacity values were measured by calculating the total Coulombic charge during Li^+ ion insertion and extraction for the charge and discharge curves, respectively.

The products were characterised by X-ray powder diffraction (Phillips PW3710-MPD with Cu Kα radiation, l = 1.54056 Å, at 40 kV (35 mA) and data was analysed using Philips X'pert XRD software). The microstructure of the electrodeposited Cu nanotubes and Cu_2O nanotubes were analysed by scanning electron microscopy (SEM) (FEI Nova 630 Nano-SEM at 15 kV).

Results and Discussion

Well ordered and homogeneous Cu nanotubes are obtained using the template mediated electrodeposition technique from $CuSO_4/H_2SO_4$ bath with the additives (PEG and Cl^-) at room temperature (13). Only when both PEG and Cl^- additives are added in the bath does the growth mechanism lead to Cu nanotubes rather than solid metallic nanowires, Figs. 2(a) and (b). The electrodeposited Cu nanotubes are converted to Cu_2O by oxygen plasma treatment. This plasma ash technique is normally used to remove organic residues after the processing in the semiconductor or packaging industries. The oxygen plasma technique was found to be efficient in the conversion of the deposited Cu in nanotube format to Cu_2O oxides. The microstructure of the Cu_2O nanotube arrays as studied by SEM as shown in Figs. 3 (a) and (b).

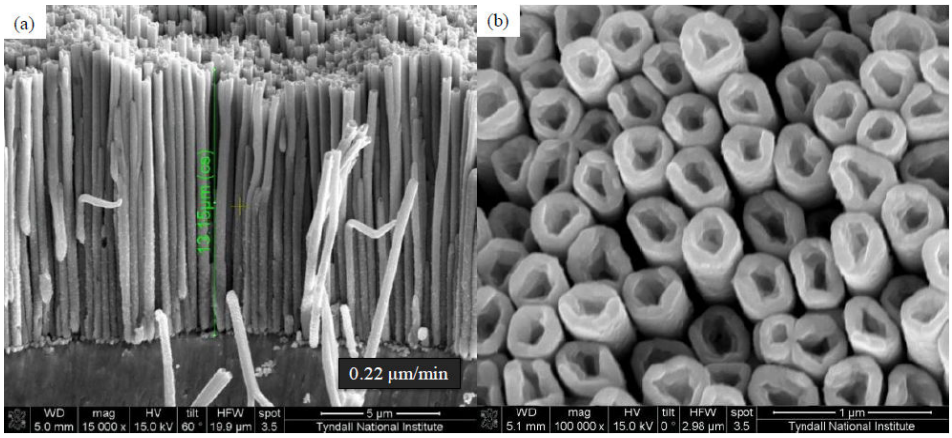


Figure 2. SEM images of as-synthesised Cu nanotube arrays, (a) cross-sectional and (b) plan views

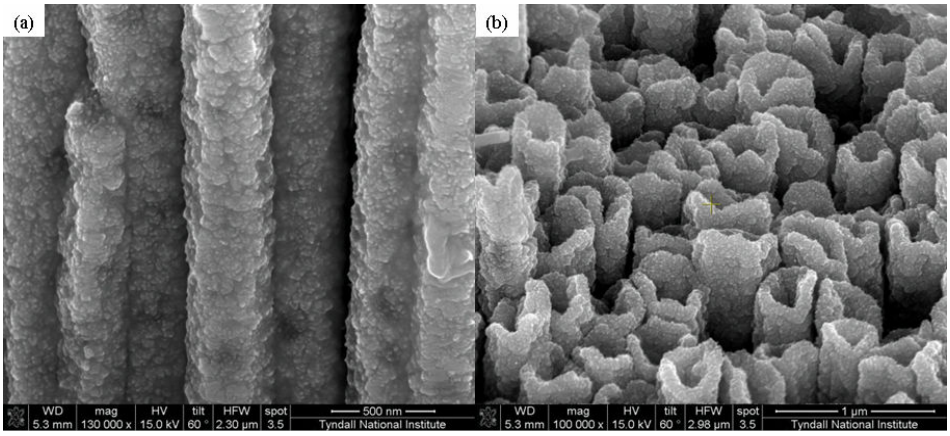


Figure 3. SEM images of the Cu_2O nanotube arrays obatined from Cu nanotubes after oxygen plasma treatment, (a) cross-sectional and b) plan view.

XRD analysis of the Cu nanotubes prior to conversion to the oxide shows a polycrystalline phase in Fig. 4(a). The crystal phase of the oxidised nanotubes is analysed by XRD as shown in Fig. 4 (b). The XRD result shows typical Cu_2O phases of 111, 200, 211, 220, 311 and 222, and also non-oxidised Cu metal phases of 100, 200 and 220. The polycrystalline nanotubes containing both Cu_2O/Cu phases clearly indicate that the metallic Cu tubes have not been completely converted to oxides during the 1 and 4.5 minutes plasma treatment at 250 W. The oxidation time at a fixed power (250 W) was varied to achieve a minimum metallic tube wall thickness as the inner core support of the outer shell oxide layers.

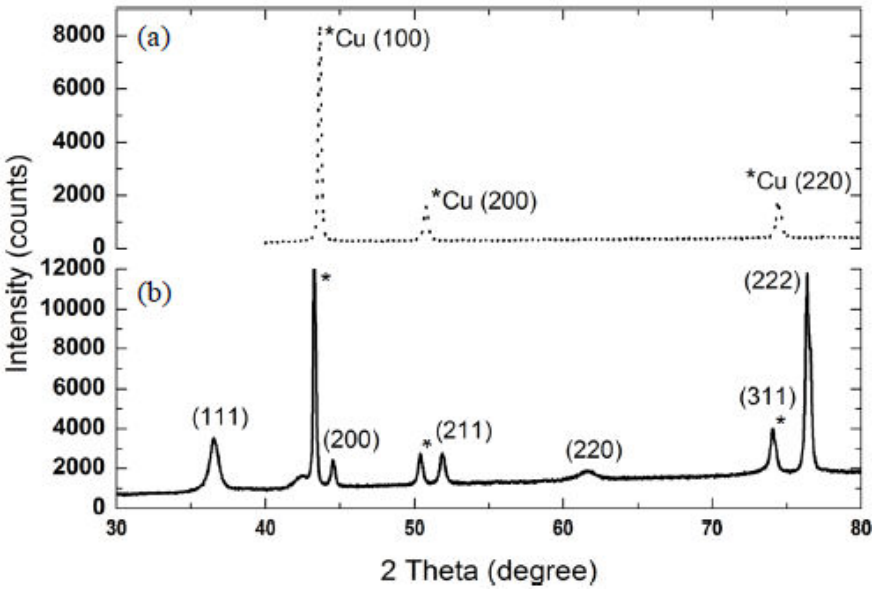


Figure 4. XRD patterns of (a) Cu nanotubes after removal of the AAO template and (b) Cu_2O nanotubes.

The conversion rates of Cu thin film and Cu nanotubes to Cu_2O are shown in Fig. 5. The electrodeposited Cu thin film and Cu nanotubes of 3 cm^2 area with 20 µm thickness were oxidised for the different intervals and the formed oxide layers were chemically removed in a commercial oxide removal solution (Schloetter S20 sulphuric acid based). The weight loss due to the oxide layer removal in this solution (Mettler Toledo XS105, repeatability (SD) = 0.02 mg) is plotted against the oxidation time in Fig. 5 (a), which gives the conversion rate plot. Then, the Cu_2O conversation rate is correlated with the wall thickness of Cu metallic tubes as shown in Fig. 5(b) e.g., for 4.1 mins plasma treatment at the specified power of 250 W the wall thickness of the Cu_2O is calculated to be 30 nm and the remaining un-oxidised Cu tube 45 nm, (given an outer tube diameter of 300 nm and inner diameter 150 nm) and assuming the Cu_2O density of 6.09 g/cm^3. The amount of Cu_2O content in Cu_2O nanotubes is estimated from the correlation curve as a function of the applied oxygen plasma treatment time.

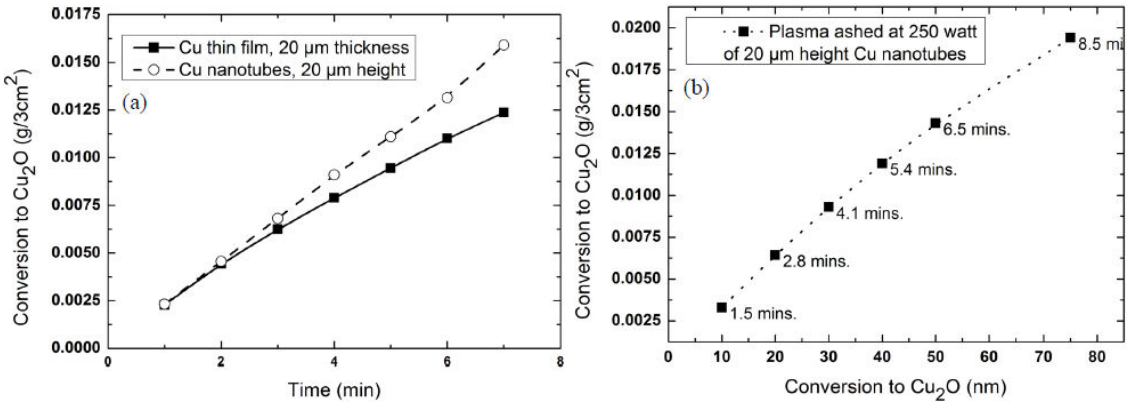


Figure 5. Conversion rate plots for Cu to Cu_2O by oxygen plasma treatment, (a) time related plot and (b) correlation plot with the wall thickness of Cu nanotubes.

The electrochemical performance of Cu_2O nanotubes was studied by cyclic voltammetry. Fig. 6(a) shows the first 20 cycles for Cu_2O nanotubes with low oxide content (~ 8 nm, or 2.32 mg / 3 cm^2, from oxygen plasma treatment for 1 min) at a sweep rate of 0.5 mV/s. In the first cycle, there is one broad cathodic peak located at 1.10 V and a small shoulder at 0.7 V, while in the following cycles three distinct cathodic reactions are observed at 1.15, 0.7 and approaching 0 V respectively. The peak at 1.10 V can be assigned to the Li^+ insertion reaction into Cu_2O and irreversible electrolyte reaction products that are not present in the second or subsequent cycles. The three regions in the following cycles are attributed to the Li^+ insertion reaction into Cu_2O crystallites (14-15). The potential of the Li^+ insertion reactions and the formation of the protective interphase layer in the first cycle are so close that they appear as a broad single peak. Meanwhile, one extended oxidation wave starting at 0.2 V up to a peak at 2.55 V corresponds to Li^+ de-insertion from the crystal lattice of Cu_2O nanotubes. It also can be seen from Fig. 6(a) that the potential of the Li^+ insertion reaction increases in the cycles following the first.

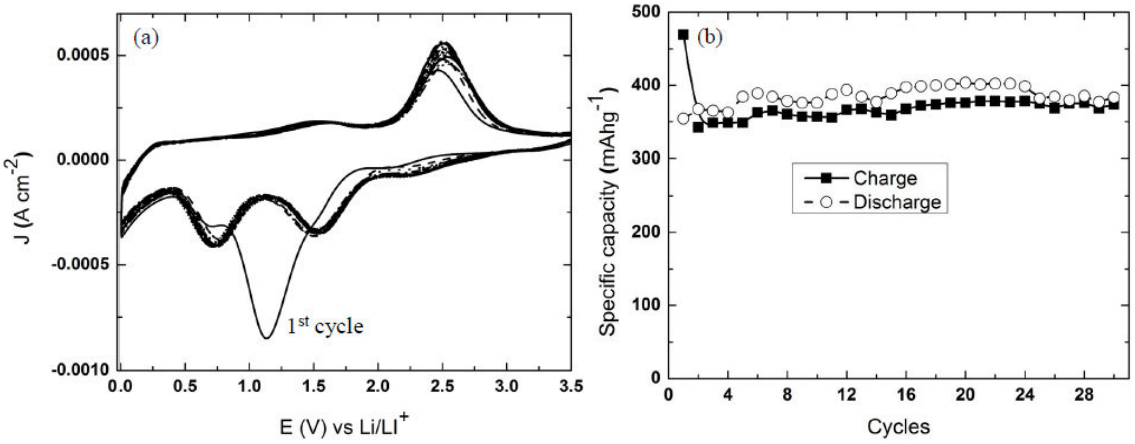


Figure 6. (a) First 20 cyclic voltammograms of Cu_2O nanotubes (low content) with sweep rate of 0.5 mV/s vs Li/Li^+, and (b) Charge-discharge capacity vs. cycle number curve of Cu_2O nanotubes for 30 cycles.

Cu_2O transfers two electrons in the electrochemical reaction and such reduction enables the conversion into nanocomposite materials consisting of nanometre scale Cu metallic clusters dispersed in an amorphous Li_2O matrix, according to the following redox reaction (5):

$$Cu_2O + 2Li^+ + 2e^- \rightarrow 2Cu + Li_2O \qquad [1]$$

The SEM image (Fig. 3a) shows that oxide morphology is not uniform along the nanotubes. At the begining of the reaction, the particle size of Cu_2O on the nanotubes is inhomogeneous. The particle size of Cu and Li_2O are assumed to be at most a few nanometres (1-5 nm) during the first charge cycle and in the following discharge cycle the reproduced Cu_2O would have the similar range of particle size as Cu and Li_2O particles formed in the first charge cycle (5). Therefore, the potential of the Li^+ insertion reaction into Cu_2O increases after the first cycle and remains constant in all the following cycles showing balanced charge-discharge behaviour. The complete overlapping of the cyclic voltammograms in continueous cycling indicates the reversibilty of Li^+ insertion

and de-insertion reactions in Cu_2O due to the homogeneous crystallites in the nanotubes. Fig. 6(b) is a charge-discharge curve of Li test in Cu_2O nanotubes by cyclic voltammetry showing the specifice Li storage capacity is still around 375 $mAhg^{-1}$ after 30 cycles with no significant deterioration. Additionally, the increased surface area of Cu_2O nanotubes due to the inner wall and the open tube end provides high electrolyte access and support for fast ionic mass transport to the remote electrode area. The high capacity retention of the self-supported Cu_2O nanotube electrodes may be attributed to the short Li^+ and e^- transport length, easy penetration of electrolyte into the pores and increased electrolytic contact area. The irreversible capacity loss in the first cycle is caused by irreversible electrolyte reactions at the Cu_2O lattice surface, which hinders lithium ion movement to the anode (16-17). These irreversible reactions are significant in nano-architectured electrodes because of the large surface and interface areas (18) but their formation decreases with cycling (19). In this work it is apparent only on the first cycle and there are no additional irreversible peaks in the cathodic sweep. The current density of 350-440 $\mu A/cm^2$ is obtained according to the cyclic voltammograms (Fig. 6a) for low content Cu_2O nanotubes, however, the current density capability would increase if they are cycled at sweep rates higher than 0.5 mV/s.

In another experiment, higher content Cu_2O nanotubes were formed by oxygen plasma treatment for 4.5 min and according to the conversion correlation curve (Fig. 5 (b)), about 34 nm of the solid Cu is converted to equilvalent Cu_2O or 10.30 mg / 3 cm^2. Fig. 7(a) shows the first three voltammograms of the Cu_2O nanotubes recorded at a sweep rate of 0.5 mV/s. These curves show the same characteristics but higher current density (1.5 mA/cm^2) as seen for low content Cu_2O electrodes at the same sweep rate. When the sweep rate is increased to 2 mV/s or 5 mV/s the current density increases but the shape of cyclic voltammograms is altered both in the cathodic or anodic regions, Fig. 7(b). At the higher sweep rate the cathodic peaks at 0.7 V and 1.15 V are a single wave until sweep reversal at 0 V while in the anodic region an oxidation peak is generated in the range of 0.5-1.0 V in addition to the peak at 2.55 V. The charge and discharge capacities in the potential range are the same as those recorded at slower sweep rates. Additionally, the polycrystalline Cu_2O particles converted to homogeneous nanparticulates with cycling may possess additional crystalline imperfections and grain boundery sites for hosting Li^+ ions. The charge-discharge capacity curves for low and high sweep rates are shown in Fig. 7(c).

At the slower sweep rate (0.5 mV/s), the charge and discharge capacity started with higher values and decreased due to the particle size effect. As mentioned in the previous section, the conversion reactions during Li^+ insertion/de-insertion produce homogeneous nanoparticles of Cu_2O, Cu and Li_2O. However, due to the higher quantity of Cu_2O a large numbers of cycles (first 20 cycles) are required to achieve uniform particles size. Once the particles size is consistent, the charge-discharge capacity increases and is stabilised from the 31^{st} cycle with slightly higher capacity (401 $mAhg^{-1}$) than that recorded for the earlier sample with thin oxide outside the Cu support. The higher specific capacity may be attributed to the presence of a large amount of Cu nanodomains during the charging process which form an interconnected network between Li_2O particles and could thereby enhance the reactivity of Li_2O reconversion to Cu_2O due to the high surface activity as well as electronic conductivity in the recharging process (5, 14).

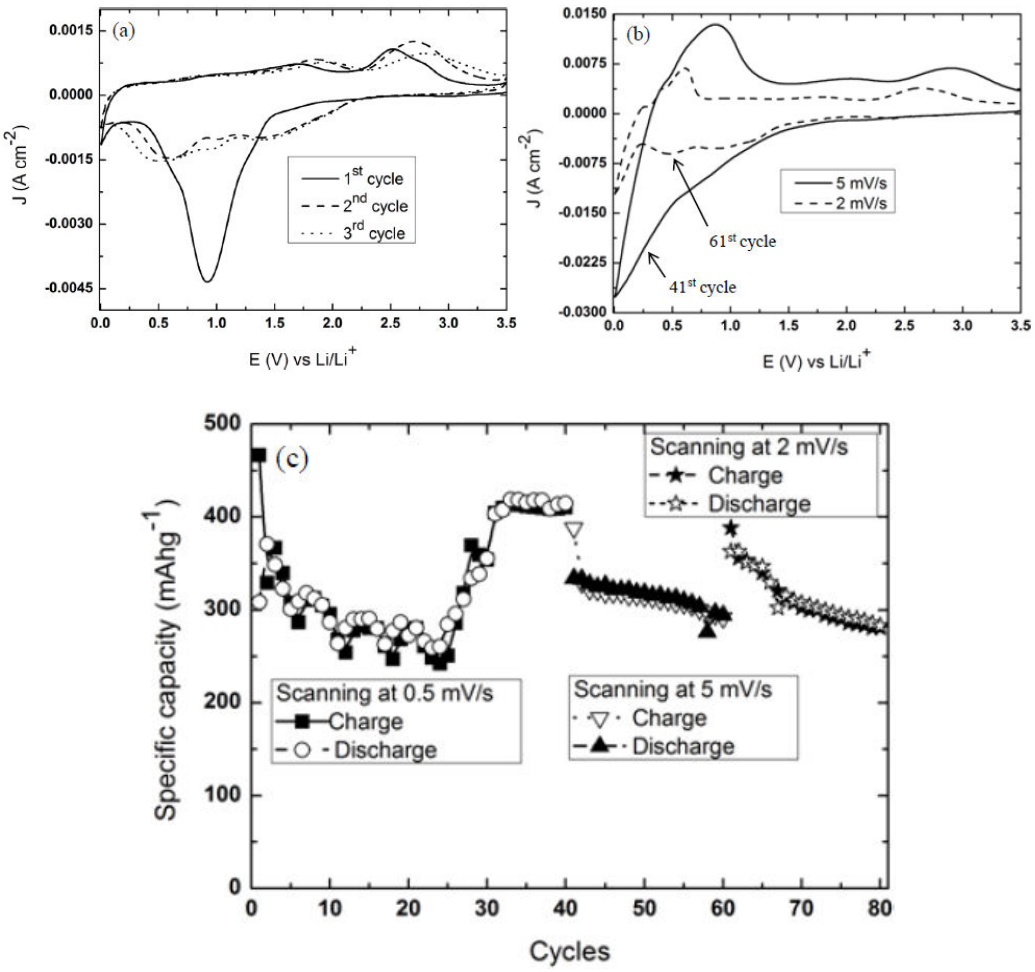


Figure 7. (a) First 3 cyclic voltammograms of Cu_2O nanotubes (higher content) with sweep rate of 0.5 mV/s vs Li/Li^+, (b) 41st and 61st cyclic voltammograms of Cu_2O nanotubes with sweep rate of 5 mV/s and 2 mV/s, respectively, vs Li/Li^+, (c) Charge-discharge capacity vs cycle number curves of Cu_2O nanotubes for 80 cycles at various sweep rates.

When the same Cu_2O nanotubes are cycled at 5 and 2 mV/s each for 20 consecutive cycles (Fig. 7(b)) the initial charging capacity (388 $mAhg^{-1}$) for both cases is consistent with the above observation for the slower sweep rate and decreases gradually (Fig. 7(c)). The slight decrease in Li^+ storage capacity of Cu_2O nanotubes may be indicative of the lower Li^+ insertion/de-insertion rates in the same potentianl intervals at higher sweep rates. The rate capability performance of Cu_2O nanotubes was measured after 80 cyclic voltammograms as described above and three charge-discharge curves at current density of 1.67 mA/cm^2, 3.33 mA/cm^2 and 5 mA/cm^2 are shown in Fig. 8 (a - c). There are three clear potential ranges at 3.0 - 1.75 V, 1.25 – 0.35 V and 0.35 – 0 V in the charge curves as shown in Fig. 8(a) and (b) consistent with three cathodic peaks in the cyclic voltammograms. The charge-discharge plateaus appear as a smooth shoulder at the current density of 5 mA/cm^2 (Fig. 8(c)). The specific capacities at 1.677 mA/cm^2 (455 $mAhg^{-1}$), 3.33 mA/cm^2 (450 $mAhg^{-1}$) and 5 mA/cm^2 (440 $mAhg^{-1}$) are quite similar for each of the current densities investigated. Therefore it is clear that the rate capability perforamance of Cu_2O nanotubes can be as high as 5 mA/cm^2 with little decrease in the available capacity of the core/shell electrode material.

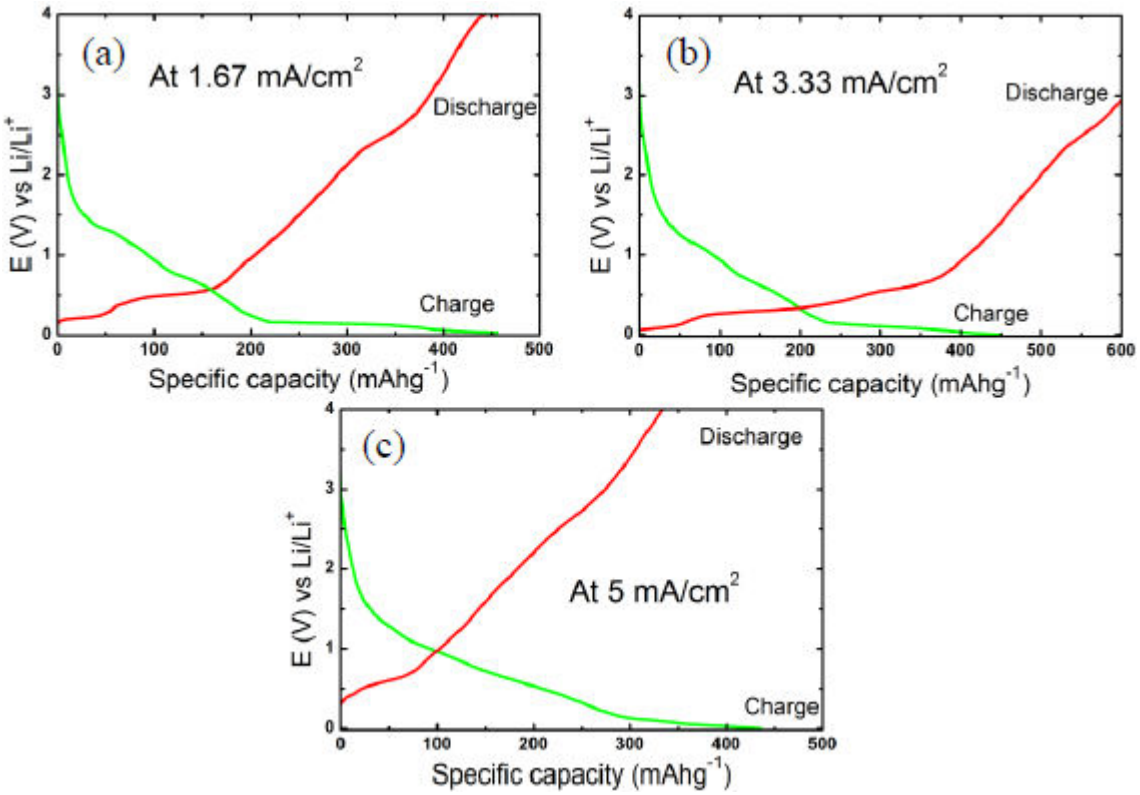


Figure 8. Charge-discharge curves of Cu_2O nanotubes started from 81st cycle at current densities of (a) 1.67 mA/cm^2, (b) 3.33 mA/cm^2 and (c) 5 mA/cm^2.

Subsequently, the same Cu_2O electrode was cycled at constant current density of 1.67 mA/cm^2 and a time limited total charge-discharge of 1 hour. Fig. 9 shows the last 11 charge–discharge curves started from 84th cycle. It can be seen from the graph that initially the charge-discharge curve reaches a potential minimum of 0 V but in later cycles reversed at approximately 0.65 V vs. Li. Initially the limited time was sufficient to utlise the full Li storage capacity (455 mAhg^{-1}) of the Cu_2O nanotubes. However, utilsation of additional capacity generated over cycling by the Cu_2O electrode required a longer cycle time. Therefore, the lower potential limit achieved during charge shifts to the more positive potential with cycling. Moreover, this electrode had experienced low and high current densities prior to this experiment which might have caused changes in nanoparticles size and structure. The cycling performances of Cu_2O nanotubes show a high level of structural integrity as capacity was retained even after 94 cycles when cycled at 1.67 mA/cm^2.

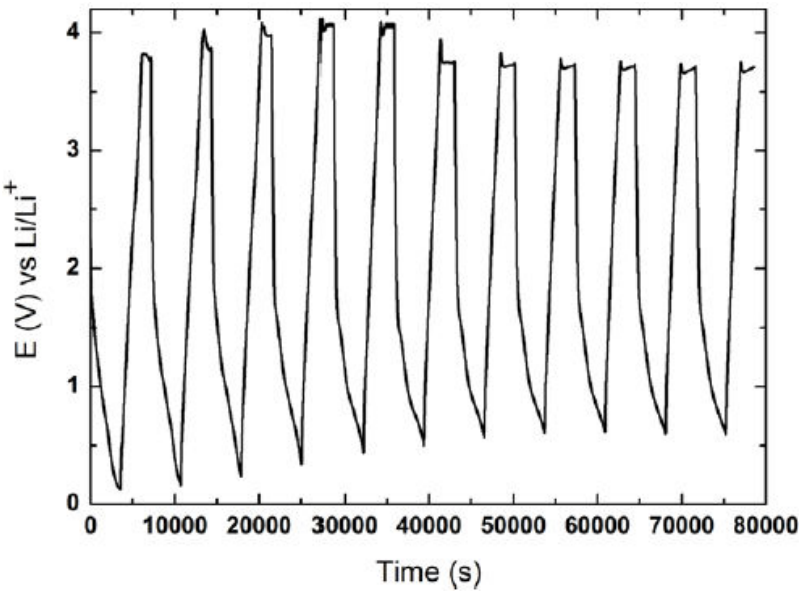


Figure 9. Charge-discharge curves of Cu_2O nanotubes started from 84th cycle at current density of 1.67 mA/cm^2 for 11 cycles.

The structural integrity and consequnt long cycleability is also supported by SEM images taken after Li cycling, see Fig. 10 (a and b). The Cu_2O nanotubes remained free standing on the substrate with uniform nanosized particles formed with cycling. The observed SEM images are consistent with the explanations given earlier for the higher capacity of Cu_2O nanotubes in terms of homogeneous nanoparticles size effects during the conversion reactions.

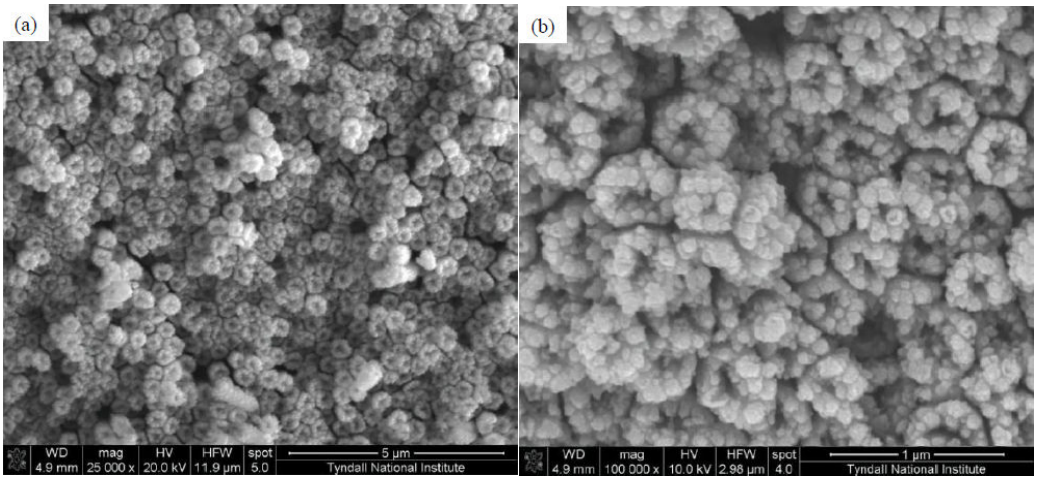


Figure 10. SEM images of Cu_2O nanotubes after 94 cycles, (a) top view and (b) high magnified top view.

To explain the enhanced cyclability of the structures reported in this work two types of Cu_2O nanotubes must be considered. We studied Cu_2O nanotubes (i) with no metallic Cu, and (ii) with metallic Cu as inner support. When Cu nanotubes are fully convereted to Cu_2O very low cycleability is observed. After 20 cycles (at 0.5 mV/s vs Li) the retention capacity is reduced to 10% of the initial value, see Fig. 11. To explain the

electron-conducting mechanism and structural integrity of Cu_2O nanotubes we propose the following, see Fig. 12 (a and b). For fully converetd Cu_2O nanotubes (Fig. 12(a)), the conversion reaction starts at the base connection with the substrate and then gradually propagates through the nanotubes. The dispersed Cu nanodomains form an interconnect network between Li_2O nanoparticles in full charged state but may not be enough to keep structural integrity of the electrode. On the other hand in the case of the Cu_2O nanotubes with metallic Cu as the inner core support with high electrical conductivity, the reaction commences along the full length of the nanotube walls (Fig. 12(b)) and structural integrity is maintained in this core(oxide)/shell(metal) type structure.

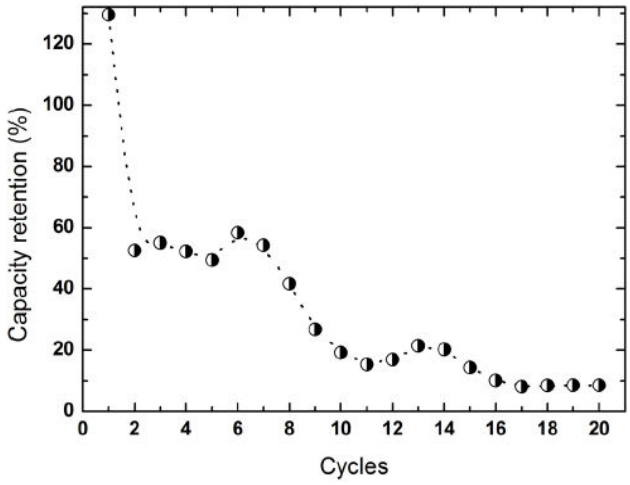


Figure 11. Capacity retention vs cycle number curve of Cu_2O nanotubes (fully converted) with sweep rate of 0.5 mV/s vs Li/Li^+.

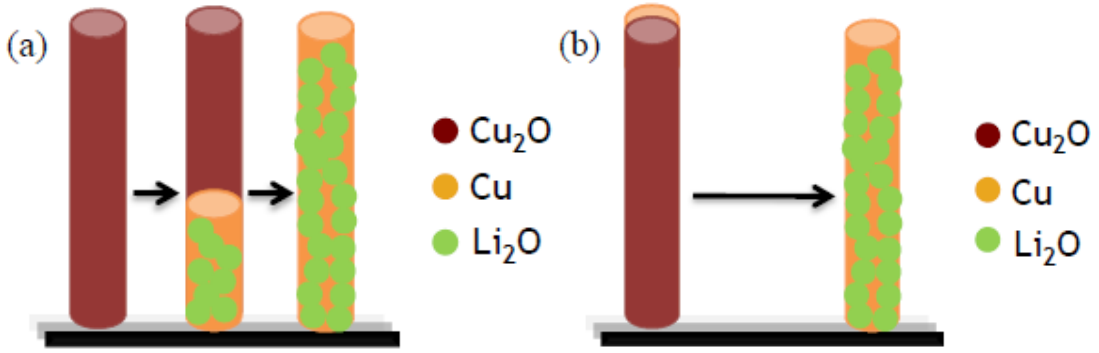


Figure 12. Schematic illustration of the electrochemical conversion reaction of Cu_2O nanotubes during charging state, (a) Cu_2O nanotubes without metallic Cu, starting from the base connection of the substarte and then gradually propagating through the nanotubes and (b) Cu_2O nanotubes with metallic Cu as inner support, commencing over the full length of the nanotube as a result of the electrical conductivity of the Cu support.

Conclusion

A direct electrodeposition technique for very high quality Cu nanotube arrays and subsequent conversion of the deposited Cu into Cu_2O has been developed. The Cu_2O nanotube arrays have shown high capacity, high cycleability and high rate capability. The cycling performance of Cu_2O nanotubes show a high level of structural integrity with capacity retention even after 94 cycles when cycled at 1.67 mA/cm^2. The outstanding electrochemical performance of the Cu_2O nanotubes comes from high surface area, easy infiltration of electrolytes, high electrical conductivity of Cu support and structural integrity. The Cu_2O nanotubes also eliminate the requirment of ancillary materials currently used in Li-ion batteries, such as carbon particles to increase conductivity.

Acknowledgment

Enterprise Ireland Technology Development Project CFTD/05/IT/317.

References

1. C. R. Sides and C. R. Martin, *Nanomaterials in Li-ion battery electrode design, Modern aspects of Electrochemistry*, No. 40, R. E. White (Ed) Springer 75 (2007).
2. A.P. Alivisatos, *Science*, **271**, 933 (1996).
3. C. Pacholski, A. Kornowsli and H. Weller, *Angew. Chem.*, Int. Ed. **41**, 1188 (2002).
4. J. H. Kim, S. Khanal, M. Islam, A. Khatri and D. Choi, *Electrochem. Commun.*, **10**, 1668 (2008).
5. P. Poizot, S. Laruelle, S. Grugeon, L. Dupont and J.-M. Tarascon, *Nature*, **407**, 496 (2000).
6. P.L. Taberna, S. Mitra, P. Poizot, P. Simon and J.-M. Tarascon, *Nature*, **5**, 567 (2006).
7. Y. Li, B. Tan and Y. Wu, *Nano Lett.*, **8**, 265 (2008).
8. S. Grugeon, S. Laruelle, R.H Urbina, L. Dupont, P. Poizot and J.-M. Tarascon, *J. Electrochem. Soc.*, **148**, A285 (2001).
9. R. Inguanta, S. Piazza and C. Sunseri, *Electrochim. Acta*, **53**, 6504 (2008).
10. S.H. Wang, Q.J. Huang, X.G. Wen, X.Y. Li, and S.H. Yang, *Phys. Chem. Chem. Phys.*, **4**, 3425 (2002).
11. A. M. Hermann, P. A. Ramkrishnan, V. Badri, P. Mardilovich and W. Landuyt, *Int. J. Hydrogen Energy*, **26**, 1295 (2001).
12. C. Mu, Y. Yu, R. Wang, K. Wu, D. Xu and G. Guo, *Adv. Mater.*, **16**, 1550 (2004).
13. T. Chowdhury, D.P. Casey and J.F. Rohan, *Electrochem. Commun.*, **11**, 1203 (2009),
14. Y.H. Lee, I.C. Leu, S.T. Chang, C.L. Liao and K.Z. Fung. *Electrochim. Acta*, **50**, 553 (2004).
15. C.Q. Zhang, J.P. Tu, X.H. Huang, Y.F. Yuan, X.T. Chen and F. Mao, *J. Alloys Compd.*, **441**, 52 (2007).
16. L.Y. Beaulieu, S.D. Beattie, T.D. Hatchard and J.R. Dahn*, J. Electrochem. Soc.*, **150,** A419 (2003).
17. N. Pereira, L.C. Klein and G.G. Amatucci, *Solid Sate Ionics*, **167**, 29 (2004).
18. H.-C. Shin and M. Liu, *Adv. Funct. Mater*, **15(4)**, 582 (2005).
19. M. Inaba, T. Uno and A. Tasaka, *J. Power Sources*, **146,** 473 (2005).